Monthly Notices
of the
ROYAL ASTRONOMICAL SOCIETY

Mon. Not. R. Astron. Soc. **412,** 1913–1925 (2011) doi:10.1111/j.1365-2966.2010.18028.x

Tracing the molecular gas in distant submillimetre galaxies via CO(1–0) imaging with the Expanded Very Large Array

R. J. Ivison,[1,2★] P. P. Papadopoulos,[3] Ian Smail,[4] T. R. Greve,[5] A. P. Thomson,[2] E. M. Xilouris[6] and S. C. Chapman[7]

[1] *UK Astronomy Technology Centre, Science and Technology Facilities Council, Royal Observatory, Blackford Hill, Edinburgh EH9 3HJ*
[2] *Institute for Astronomy, University of Edinburgh, Blackford Hill, Edinburgh EH9 3HJ*
[3] *Argelander-Institüt für Astronomie, Auf dem Hügel 71, D-53121, Germany*
[4] *Institute for Computational Cosmology, Durham University, South Road, Durham DH1 3LE*
[5] *Dark Cosmology Centre, Niels Bohr Institute, University of Copenhagen, Juliane Maries Vej 30, 2100 Copenhagen Ø, Denmark*
[6] *Institute of Astronomy and Astrophysics, National Observatory of Athens, I. Metaxa and Vas. Pavlou Streets, P. Penteli, GR-15236 Athens, Greece*
[7] *Institute of Astronomy, University of Cambridge, Madingley Road, Cambridge CB3 0HA*

Accepted 2010 November 15. Received 2010 November 2; in original form 2010 September 2

ABSTRACT

We report the results of a pilot study with the Expanded Very Large Array (EVLA) of ^{12}CO $J = 1$–0 emission from four submillimetre-selected galaxies at $z = 2.2$–2.5, each with an existing detection of ^{12}CO $J = 3$–2, one of which comprises two distinct spatial components. Using the EVLA's most compact configuration, we detect strong, broad [medians: 990 km s^{-1} full width at zero intensity; 540 km s^{-1} full width at half-maximum (FWHM)] $J = 1$–0 line emission from all of our targets – coincident in position and velocity with their $J = 3$–2 emission. The median linewidth ratio, $\sigma_{1-0}/\sigma_{3-2} = 1.15 \pm 0.06$, suggests that the $J = 1$–0 is more spatially extended than the $J = 3$–2 emission, a situation confirmed by our maps which reveal velocity structure in several cases and typical sizes of ∼16 kpc FWHM. The median brightness temperature (T_b) ratio is $r_{3-2/1-0} = 0.55 \pm 0.05$, consistent with local galaxies with $L_{IR} > 10^{11}\,L_\odot$, noting that our value may be biased high because of the $J = 3$–2 based sample selection. Naively, this suggests gas masses roughly two times higher than estimates made using higher J transitions of CO, with the discrepancy due entirely to the difference in assumed T_b ratio. We also estimate molecular gas masses using the ^{12}CO $J = 1$–0 line and the observed global T_b ratios, assuming standard underlying T_b ratios for the non-star-forming and star-forming gas phases as well as a limiting star formation efficiency for the latter in all systems, i.e. without calling upon X_{CO} ($\equiv \alpha$). Using this new method, we find a median molecular gas mass of $(2.5 \pm 0.8) \times 10^{10}\,M_\odot$, with a plausible range stretching up to three times higher. Even larger masses cannot be ruled out, but are not favoured by dynamical constraints: the median dynamical mass within $R \sim 7$ kpc for our sample is $(2.3 \pm 1.4) \times 10^{11}\,M_\odot$ or ∼6 times more massive than UV-selected galaxies at this epoch. We examine the Schmidt–Kennicutt (S–K) relation for all the distant galaxy populations for which CO $J = 1$–0 or $J = 2$–1 data are available, finding small systematic differences between galaxy populations. These have previously been interpreted as evidence for different modes of star formation, but we argue that these differences are to be expected, given the still considerable uncertainties, certainly when considering the probable excitation biases due to the molecular lines used, and the possibility of sustained S–K offsets during the evolution of individual gas-rich systems. Finally, we discuss the morass of degeneracies surrounding molecular gas

★E-mail: rji@roe.ac.uk

mass estimates, the possibilities for breaking them, and the future prospects for imaging and studying cold, quiescent molecular gas at high redshifts.

Key words: galaxies: evolution – galaxies: high-redshift – galaxies: starburst – infrared: galaxies – radio lines: galaxies – submillimetre: galaxies.

1 INTRODUCTION

The star formation density contributed by ultraluminous infrared galaxies (ULIRGs) appears to increase out to $z \gtrsim 2$ (e.g. Chapman et al. 2005; Wardlow et al. 2010). These galaxies are often heavily obscured by dust and hence the bulk of their luminosity is radiated in the rest-frame far-infrared (far-IR) and observed in the submillimetre (submm) band, hence their epithet: 'submm galaxies' (SMGs). SMGs have the potential to form the stellar mass of an L^* galaxy in a single event (e.g. Lilly et al. 1999; Smail et al. 2004; Swinbank et al. 2006; Hainline et al. 2010). To accomplish this feat, however, SMGs must have sufficiently large reservoirs of cold gas, $\gtrsim 10^{11}\,M_\odot$. The first searches for molecular gas emission, via the $J = 3$–2 or 4–3 transitions of ^{12}CO, were successful in detecting significant quantities of gas in several SMGs (Frayer et al. 1998, 1999; Ivison et al. 2001). Subsequent, larger surveys with the Plateau de Bure Interferometer (PdBI) greatly expanded this work (e.g. Downes & Solomon 2003; Genzel et al. 2003; Kneib et al. 2005; Greve et al. 2005; Tacconi et al. 2006; Bothwell et al. 2010).

Observations of the molecular gas within high-redshift galaxies provide powerful insight into the physics of star formation in these systems (Solomon & Vanden Bout 2005), and allow comparisons with local systems. More specifically they allow us to (i) probe the mass and extent of the reservoir of molecular gas available for fuelling their prodigious starbursts, (ii) determine the dynamical mass of the host galaxy, free from the uncertainties arising from outflows and patchy dust extinction which plagues optical and near-IR spectroscopic studies (e.g. Swinbank et al. 2006; Ivison et al. 2010a) and (iii) derive their gas-mass fraction, $M_{\rm gas}({\rm H_2})/M_{\rm dyn}$. The dynamical mass is a strong indicator of the 'end' state of such systems in the present Universe, while a well-determined gas-mass fraction indicates their likely evolutionary status at the look-back time where they are observed. Finally, gas-consumption time-scales, $\langle\tau_{\rm gas}\rangle = M({\rm H_2})/{\rm SFR}$, where SFR is the star-formation rate, give the minimum time-scale for the conclusion of their star-forming (SF) episodes.

While the PdBI studies of SMGs represent a considerable advance, they are fundamentally limited by their focus on high-J ^{12}CO lines whose high excitation requirements ($n_{\rm crit} \sim 10^4$–$10^5\,{\rm cm^{-3}}$, $E_{\rm u}/k_{\rm B} \sim 50$–$150\,{\rm K}$) confine the emission from such transitions to regions of active star formation, rather than tracing the total available reservoir of gas within a galaxy. In the nearby archetypal starburst, M 82, such lines would reveal only the highly excited, SF molecular gas in its inner 400 pc (Mao et al. 2000; Weiß et al. 2001) rather than the more massive, low-excitation gas component that extends ∼1.7 kpc beyond its centre (Walter, Weiss & Scoville 2002; Weiß, Walter & Scoville 2005b). This also suggests potential spatial biases in the high-J ^{12}CO emission – which exhibit typical half-light radii of 0.8–2.8 kpc for SMGs (Tacconi et al. 2008) – means they may not trace the true dimensions (or kinematics) of the total molecular gas distribution.

A recent comparison of ^{12}CO line ratios between local, IR-luminous galaxies and distant SMGs has provided strong indications that several high-redshift systems must contain significant amounts of colder, non-SF gas or – for a few compact, extreme starbursts – that they may suffer high optical depths at short submm wavelengths due to dust (Papadopoulos, Isaak & van der Werf 2010b). Thus their high-J ^{12}CO line emission may not be a good tracer of the total CO-rich molecular gas mass, its distribution, or the total enclosed dynamical masses, as is usually assumed (e.g. Tacconi et al. 2006). Indeed the low brightness temperature ($T_{\rm b}$) ratios of ^{12}CO $J = 7$–6 (or 6–5) to 3–2 ($r_{7-6/3-2} \lesssim 0.3$) measured in several SMGs (Tacconi et al. 2006) *are not* typical of dense, warm, SF gas providing strong but still circumstantial evidence that high-J ^{12}CO line studies may miss a critical gas component in SMGs.

The earliest evidence of low, Milky Way type, global CO line excitation in a distant SF system was uncovered in the submm-bright extremely red object, HR 10 (Papadopoulos & Ivison 2002). Since then a handful of SMGs have been observed in ^{12}CO $J = 1$–0 (Greve, Ivison & Papadopoulos 2003; Hainline et al. 2006; Carilli et al. 2010; Frayer et al. 2010; Harris et al. 2010; Ivison et al. 2010a; Swinbank et al. 2010), and several show evidence of substantial reservoirs of ^{12}CO $J = 1$–0 with $r_{3-2/1-0} \sim 0.5$ (see also Danielson et al. 2010). A systematic underestimate of molecular gas mass via high-J CO line emission could lie at the heart of the apparent discrepancy between the gas-depletion time-scales for SMGs, 40–100 Myr, based on high-J observations (Greve et al. 2005), and the proposed lifetimes of these luminous starbursts, ∼300 Myr (Swinbank et al. 2006, 2008), though strong feedback events will punctuate the evolutionary path of any starburst and these are expected to lengthen any putative gas-consumption times-scales. This, in turn, influences our understanding of the evolutionary links between SMGs and other high-redshift populations, e.g. quasars or passive galaxies (Chapman et al. 2005; Wardlow et al. 2010) which rely on duty-cycle and space–density arguments, which then influences our interpretation of their likely descendants at $z \sim 0$ (Swinbank et al. 2008). Similarly, the spatial bias in the high-J ^{12}CO dynamical tracers employed for SMGs means we might be missing important signatures in the velocity fields at large radii, perhaps reflecting disc-like rotation or even evidence for cold-flow accretion (e.g. Dekel, Sari & Ceverino 2009).

To address these concerns, we have undertaken a pilot study with the National Radio Astronomy Observatory's (NRAO)[1] Expanded Very Large Array (EVLA) of ^{12}CO $J = 1$–0 emission from four well-studied SMGs, with $S_{850\,\mu{\rm m}} \sim 10\,{\rm mJy}$ at $z = 2.2$–2.5, two each in the Great Observatories Origins Surveys (GOODS) North and European Large Area Infrared Survey (ELAIS) N2 submm survey fields (Scott et al. 2002; Borys et al. 2003), pinpointed accurately via arcsec-resolution radio continuum imaging[2] (Ivison et al.

[1] NRAO is operated by Associated Universities Inc., under a cooperative agreement with the National Science Foundation.

[2] The ELAIS N2 continuum image was recreated from the raw data (programmes AI91 and AD432) to avoid the astrometric issue described by Morrison et al. (2010). See also http://science.nrao.edu/evla/archive/issues/#010.

2002; Chapman et al. 2005), with redshifts determined via Keck spectroscopy (Chapman et al. 2003, 2005) and confirmed via detections of ^{12}CO $J = 3$–2 at PdBI (Neri et al. 2003; Greve et al. 2005; Tacconi et al. 2006, 2008). Ultimately, the combination of EVLA and PdBI imaging will allow us to compare the gas masses, morphologies and dynamics derived from the ^{12}CO $J = 1$–0 and 3–2 or higher-J lines in these intense starbursts. In this first paper, we explore those parameters probed by the initial phase of our EVLA survey, conducted at relatively low resolution using the EVLA's most compact configuration during shared-risk time.

Throughout the paper, we use a cosmology with $H_0 = 71\,\mathrm{km\,s^{-1}\,Mpc^{-1}}$, $\Omega_\mathrm{m} = 0.27$, $\Omega_\Lambda = 0.73$, which gives a median angular scale of 8.2 kpc arcsec^{-1} for our sample.

2 OBSERVATIONS AND DATA REDUCTION

Our sample was chosen such that the ^{12}CO $J = 1$–0 line is redshifted to the ∼33–36 GHz frequency range, where both sub-band pairs of the EVLA's new K_a-band receivers can be utilized, yielding up to 256 MHz of instantaneous bandwidth during the earliest shared-risk phase of EVLA commissioning with the new Wideband Interferometric Digital Architecture (WIDAR) correlator (see Table 1). We overlapped the two 64 × 2 MHz dual-polarization sub-bands by a total of 10 channels – to minimize issues with the edge channels – and we centred the lines 36 MHz to the red, using the redshifts published by Tacconi et al. (2006, 2008). This latter precaution proved unnecessary. Our approach ultimately yielded a single 236-MHz data set for each target, ∼2000 km s^{-1} of coverage with 16.7–18.2 km s^{-1} channels, covering $uv \sim 5$–100 kλ.

Each target was observed for between five and seven 3-h tracks during 2010 April–July (Table 1), a period during which ∼15 functional K_a-band receivers were typically available and the EVLA was in its most compact configuration (D), recording data every 1 s, with a resultant data rate of ∼6.3 GB h^{-1} (programme AS1013). The tracks were scheduled flexibly to ensure appropriate weather conditions for these high-frequency observations. After 2010 May 12, several antennas were plagued by phase jumps, but most of these data were salvaged. Three tracks suffered severe phase jumps or unsuitable weather and were discarded. Antenna pointing was checked every 90 min at 5 GHz. Each track contained a 5-min scan of 1331+305 (3C 286) for absolute flux calibration (1.87 Jy at 35.1 GHz), and regular (every $\lesssim$5 min) scans of the bright, local calibrators, 1302+575 and 1642+394 (∼0.35 and ∼7.0 Jy, respectively). The latter has been monitored at 33.75 GHz (Davies et al. 2009), and we found consistent flux densities when bootstrapping from 0137+331, albeit with evidence of the variability found by Franzen et al. (2009).

Editing and calibration were accomplished within AIPS (31DEC10). For 1331+305, we used an appropriately scaled 22.5-GHz model to determine gain solutions; the other calibrators were used to determine the spectral variation of the gain solutions (the 'bandpass'), after first removing atmospheric phase drifts on a time-scale of 6–12 s via self-calibration with a simple point-source model. Despite the significant increase in data volume relative to the old VLA correlator, we were able to employ standard AIPS recipes throughout the data-reduction process.

3 RESULTS

3.1 Infrared luminosities

On several occasions in the subsequent discussion, e.g. Sections 4.3, 4.5 and 4.6, we shall call upon SFRs determined from rest-frame 8–1000 μm luminosities, L_IR, so we start by describing these measurements.

For our SMGs, plus 13 others available in the literature with measurements of ^{12}CO $J = 1$–0 or $J = 2$–1 and comparable selection biases and general properties (Greve et al. 2003, 2005; Hainline et al. 2006; Frayer et al. 2008; Schinnerer et al. 2008; Knudsen et al. 2009; Ivison et al. 2010a,b; Harris et al. 2010; Carilli et al. 2010; Swinbank et al. 2010), we derive L_IR by fitting the spectral energy distribution (SED) template from Pope et al. (2008) and that of SMM J2135−0102 (Swinbank et al. 2010; Ivison et al. 2010b) to the available photometric data, ignoring the radio photometry for those sources known to suffer contamination by active galactic nucleus (AGN): SMM J163650 (Smail et al. 2003), SMM J02399 (Ivison et al. 2010a) and SMM J14009 (Ivison et al. 2000; Weiß et al. 2009). The SMM J2135 SED gave better fits, and we adopt these values, which are 10–20 per cent higher than those given by the Pope et al. (2008) template. We then convert these into SFRs, following Kennicutt (1998a). Our five SMGs have a mean L_IR of $(5.4 \pm 0.8) \times 10^{12}\,\mathrm{L_\odot}$ (see Table 3) and a corresponding SFR of $930 \pm 140\,\mathrm{M_\odot\,yr^{-1}}$ (for the full sample, $L_\mathrm{IR} = (5.5 \pm 0.9) \times 10^{12}\,\mathrm{L_\odot}$ and $950 \pm 155\,\mathrm{M_\odot\,yr^{-1}}$).

3.2 Spectra and morphologies

We construct maps of each source, stepping through the frequency range of the data, examining image cubes with velocity resolutions ranging from 2 to 16 channels (35–250 km s^{-1}). The synthesized beam for a natural weighting scheme is typically 2.7×2.0 arcsec^2 with a position angle (PA) near −5°, or 3.2×2.6 arcsec^2 when employing a Gaussian taper that reaches 30 per cent at 80 kλ. We find strong ^{12}CO $J = 1$–0 line emission from each of the four SMGs, at the expected positions and frequencies derived from the ^{12}CO $J = 3$–2 emission, though we note that some published redshifts/spectra are misleading – e.g. for SMM J123707, Tacconi et al. (2006) quote $z = 2.490$ rather than $z = 2.486$. We see two distinct spatial components in SMM J123707, so we hereafter refer to a sample of five SMGs using the suffixes -NE and -SW for SMM J123707,

Table 1. SMG sample and observing log.

Target name SMM J...	$z_{\mathrm{CO3–2}}$ [a]	Deboosted $S_{850\,\mu\mathrm{m}}$ (mJy)	$S_{1.4\,\mathrm{GHz}}$ (μJy)	Observing dates (2010) (2.0–2.1 h per track, on-source)	Alternative target names
123549.44+621536.8	2.202	8.3 ± 2.5	81 ± 5	May 2, 14, 15, 16, Jun 20, 27, Jul 6	HDF 76
123707.21+621408.1-NE	2.486	10.7 ± 2.7	39 ± 8	Apr 12, 14, 22, May 4, 6	HDF 242, GN 19
123707.21+621408.1-SW			30 ± 8		
163650.43+405734.5	2.385	8.2 ± 1.7	242 ± 11	Apr 16, 19 (× 2), 20, May 8, 11, 12	N2 850.4, N2 1200.10
163658.19+410523.8	2.452	10.7 ± 2.0	115 ± 11	Apr 22, 27, May 8, 14, Jun 20, 21, Jul 7	N2 850.2

[a]CO $J = 3$–2 redshifts from Tacconi et al. (2006); for SMM J123707, we quote the value used to determine velocities in that work.

following Tacconi et al. (2006). We extract a spectrum for the emission in an area corresponding to around three synthesized beams, centred on each of our targets (SMM J123707-NW and -SW are combined in this case) and show these in Fig. 1, after Hanning smoothing with a four-channel triangular kernel. All sources display broad lines, with full width at zero intensity (FWZI) of $\sim$1000 km s^{-1}. We measure the line fluxes by integrating the emission across the velocity ranges reported in Table 1 (no continuum correction is applied as we detect no significant continuum emission from any of the SMGs, $3\sigma < 60$ μJy, as expected). We assess the uncertainty in the velocity-integrated fluxes from the variance of the off-line emission, and we report the flux and associated error in Table 2. We also list the CO $J = 3$–2 line intensities (from Tacconi et al. 2008) for our five SMGs, having checked for consistency with the low-resolution fluxes of Greve et al. (2005).

We calculate the intensity-weighted redshift for the emission in the velocity window and report this in Table 2. It is clear from Tacconi et al. (2008) that some of the ^{12}CO $J = 3$–2 lines are better fit by two Gaussian profiles and this is also true for several of the ^{12}CO $J = 1$–0 lines; however, for the sake of uniformity we determine the intensity-weighted second moment of the velocity distribution and report this as the equivalent 1σ width of a Gaussian with the same second moment in Table 2. We find a median full width at half-maximum (FWHM) of 540 ± 110 km s^{-1} for our target SMGs, which is nearly double the median FWHM of 300 ± 20 km s^{-1} measured for the ^{12}CO $J = 1$–0 emission in ULIRGs by Solomon et al. (1997). For comparison, we also calculate the equivalent 1σ width of the ^{12}CO $J = 3$–2 emission in the same velocity range from the spectra shown in Tacconi et al. (2008), finding a median ratio between the two linewidths of $\sigma_{1-0}/\sigma_{3-2} = 1.15 \pm 0.06$. Assuming that the dynamics of the central regions of these systems are dominated by baryonic gas discs, then this suggests that the ^{12}CO $J = 1$–0 is more spatially extended than the ^{12}CO $J = 3$–2 emission, a situation confirmed by our maps.

Fig. 1 also shows the maps of the ^{12}CO $J = 1$–0 emission. We mark the centroids of the ^{12}CO $J = 3$–2 emission for all of the sources, confirming that the ^{12}CO $J = 1$–0 emission is spatially coincident in all cases, although we note that in SMM J163658 there is evidence that the 1.4-GHz continuum is offset to the north of the $J = 3$–2 emission which is, in turn, offset to the north of the $J = 1$–0 centroid – a situation reminiscent of the complex AGN/starburst, SMM J02399−0136 (Ivison et al. 2010a).

Even though these ^{12}CO $J = 1$–0 maps were taken with the most compact EVLA configuration, they resolve all of the systems except SMM J123707-SW, one of two ^{12}CO $J = 1$–0 emitters separated by $\sim$3 arcsec ($\sim$23 kpc) in the field of SMM J123707, as previously identified in ^{12}CO $J = 3$–2 with PdBI and at 1.4 GHz with the VLA by Tacconi et al. (2006). The north-eastern component within SMM J123707 and the other three SMGs have typical FWHM of $\sim$2 arcsec or $\sim$16 kpc. These sizes are larger than the 0.8–2.8 kpc half-light radii deduced from the higher J transitions by Tacconi et al. (2008), as expected from the larger linewidths. Combining our data with the forthcoming C-configuration EVLA observations of ^{12}CO $J = 1$–0 will ensure we have sufficient sensitivity and resolution to confirm this suggestion.

We also find evidence for velocity structure within several of the sources. In SMM J123549, we identify a northern spur to the $J = 1$–0 emission (see inset, Fig. 1), centred at -150 km s^{-1}, which is not seen in $J = 3$–2. This feature is coincident with a prominent, narrow feature in the $J = 1$–0 spectrum and suggests that the system may contain two components (cf. 4C 60.07; Ivison et al. 2008). We find a velocity difference of just 80 ± 60 km s^{-1} between the two components of SMM J123707, suggesting that they are orbiting one another in the plane of the sky with a physical separation of $\sim$25 kpc. We also see velocity structure within SMM J123549 and most strikingly a velocity gradient of $\sim$600 km s^{-1} across SMM J123707-NE over a spatial scale of $\sim$2 arcsec ($\sim$16 kpc – see inset, Fig. 1), though our spatial resolution is currently insufficient to determine whether the velocity structure is well ordered.

3.3 Brightness temperature ratios: average gas excitation

Combining our new ^{12}CO $J = 1$–0 data with the ^{12}CO $J = 3$–2 luminosities from Tacconi et al. (2008), we derive a weighted-mean T_b ratio of $r_{3-2/1-0} = 0.56 \pm 0.05$ (the median ratio and bootstrapped error are 0.55 ± 0.05). Including similar observations of the same transitions in the five $z \sim 2$ SMGs from Ivison et al. (2010a), Harris et al. (2010) and Swinbank et al. (2010), we derive a weighted-mean T_b ratio of $r_{3-2/1-0} = 0.65 \pm 0.02$ and a median of 0.58 ± 0.05. The distributions of $r_{3-2/1-0}$ for our sample and the literature sources are statistically indistinguishable.

The weighted-mean T_b ratio for the Yao et al. (2003) subsample of local IR-luminous galaxies with rest frame 8–1000 μm luminosities, $L_{IR} \geq 10^{11}$ L$_\odot$, is $r_{3-2/1-0} = 0.57 \pm 0.06$ with a median of 0.63 ± 0.10, similar to that of high-redshift SMGs (see also Harris et al. 2010). This is also consistent with the average excitation conditions of local LIRGs studied by Yao et al., but L_{IR} and the molecular gas mass is typically an order of magnitude larger for the SMGs. This similarity, while reassuring, does not mean that the physical state of the molecular gas in SMGs and LIRGs is identical. Indeed, $r_{3-2/1-0}$ is often low for the LIRGs studied by Yao et al., which is atypical of dense, SF molecular gas (where this ratio would approach unity); this is thought to be caused by a diffuse, unbound, warm gas phase that is frequently found in galactic nuclei. The physical scale sampled by our beam in SMGs at $z \sim 2.4$ ($\sim$20 kpc) is larger than that employed for the LIRGs studied by Yao et al. ($\sim$2–6 kpc) and may sample an extended, cold molecular gas phase that can suppress the global $r_{3-2/1-0}$ (an issue discussed in detail in Section 4.3).

We highlight two features of our $r_{3-2/1-0}$ distribution. First, we are using what is effectively a ^{12}CO $J = 3$–2 selected sample for this analysis, and it is possible that SMGs with lower $r_{3-2/1-0}$ ratios remained undetected by the ^{12}CO $J = 3$–2 surveys and were thereby excluded from our study. We note that a programme to search for ^{12}CO $J = 1$–0 emission using the Zpectrometer instrument on the Green Bank Telescope (GBT) from SMGs which were undetected in ^{12}CO $J = 3$–2 by PdBI has been terminated due to problems with GBT's K_a receiver. Secondly, we stress that there is a wide range in the apparent $r_{3-2/1-0}$ values within the SMG sample but that formally these are consistent with our error-weighted mean value, given the quoted uncertainties, so we have yet to uncover the variation in $r_{3-2/1-0}$ seen locally (Yao et al. 2003).

3.4 The plausible range of molecular gas masses

The key advantage of observing the lowest ^{12}CO $J = 1$–0 transition is that it allows us to determine their molecular gas mass and its distribution in a manner identical to that used in the local Universe, which permits a direct comparison of these systems to local IR-luminous galaxies. A firm lower limit on the molecular gas mass can be obtained by assuming local thermodynamic equilibrium and

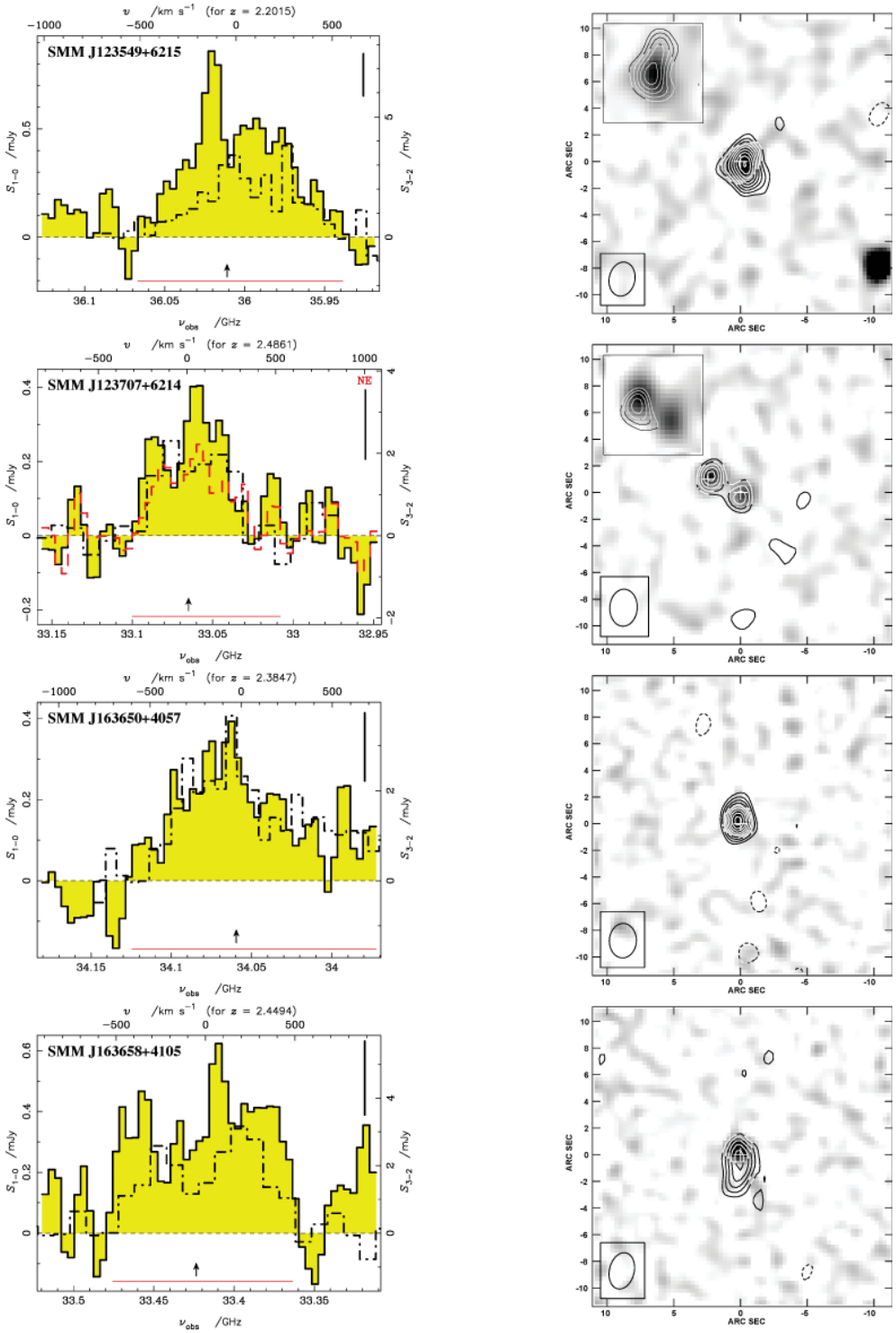

Figure 1. CO $J = 1$–0 spectra and lightly CLEANed images for the SMGs in our study. On the left we show the spectra, integrated over a region of ∼3 beam areas in the data cubes, with the corresponding PdBI CO $J = 3$–2 spectra from Tacconi et al. (2006) shown as dot–dashed lines, scaled by 9^{-1} times to be on the same Rayleigh–Jeans T_b scale. Arrows indicate the CO $J = 3$–2 line centres. The CO $J = 1$–0 spectrum of the NE component of SMM J123707 is shown in red. All our targets are well detected with CO $J = 1$–0 FWHM of ∼300–800 km s^{-1}, marginally broader than the corresponding CO $J = 3$–2 emission. The frequency range used to create the images in the right-hand panels are indicated below each spectrum. A typical $\pm 1\sigma$ error bar is shown at the top right of each panel. Velocities are relative to the CO $J = 1$–0 redshifts listed in Table 2 and the spectra have been Hanning smoothed with an four-channel triangular kernel with 4-MHz (∼35 km s^{-1}) spectral resolution. Right: CO $J = 1$–0 emission integrated over the channels indicated in the corresponding spectrum, displayed as contours (-3, 3, 4... $\times\ \sigma$ where σ is typically ∼20 μJy beam^{-1}), superimposed on linear grey-scales of the 1.4-GHz continuum emission. We see that all targets are marginally or well resolved at the resolution of our map, with SMM J123707 comprising two components. The beam is shown in the bottom left corner of each image. Insets show 6×6 arcsec^2 postage stamps of CO $J = 1$–0 for SMM J123549 (a 220-km s^{-1} wide bin centred at -150 km s^{-1}, displayed as contours, superimposed on a grey-scale of the total CO $J = 1$–0 emission) and SMM J123707 (contiguous 390-km s^{-1} wide blue and red bins represented by the contours and the underlying grey-scale, respectively, illustrating the velocity gradient across SMM J123707-NE).

Table 2. SMG observed properties.

Name	$z_{\rm CO(1-0)}$	I_{1-0} (Jy km s^{-1})	I_{3-2} (Jy km s^{-1})	$r_{3-2/1-0}$	$r_{6-5/3-2}$	$(\sigma_{1-0})^a$ (km s^{-1})	FWZI (km s^{-1})	R (kpc)
SMM J123549	2.2015 ± 0.0002	0.32 ± 0.04	1.6 ± 0.2	0.56 ± 0.10	0.36 ± 0.08	230 ± 20	1050	7 ± 2
SMM J123707-NE	2.4870 ± 0.0005	0.09 ± 0.02	0.32 ± 0.09	0.40 ± 0.14	–	200 ± 35	830	7 ± 2
SMM J123707-SW	2.4861 ± 0.0004	0.12 ± 0.02	0.59 ± 0.09	0.55 ± 0.12	–	140 ± 30	920	<3
SMM J163650	2.3847 ± 0.0004	0.34 ± 0.04	2.3 ± 0.3	0.75 ± 0.13	0.23 ± 0.05	330 ± 35	1340	6 ± 2
SMM J163658	2.4494 ± 0.0002	0.37 ± 0.07	1.8 ± 0.2	0.54 ± 0.12	0.33 ± 0.07	295 ± 10	990	11 ± 3

[a] FWHM $= 2\sqrt{2\ln 2} \times \sigma$.

an optically thin transition where

$$\frac{M({\rm H_2})}{L'_{\rm CO1-0}} = X_{\rm CO}^{\rm thin} \sim 0.08 \left[\frac{g_1}{Z}\, {\rm e}^{-T_\circ/T_{\rm k}} \left(\frac{J(T_{\rm k}) - J(T_{\rm bg})}{J(T_{\rm k})} \right) \right]^{-1} \times \left(\frac{[{\rm CO/H_2}]}{10^{-4}} \right)^{-1} \frac{{\rm M_\odot}}{{\rm K\,km\,s^{-1}\,pc^2}}, \quad (1)$$

with $T_\circ = E_{\rm u}/k_{\rm B} \sim 5.5$ K, $J(T) = T_\circ({\rm e}^{T_\circ/T} - 1)^{-1}$, $T_{\rm bg} = (1 + z)\, T_{\rm CMB} = 9.52$ K (the temperature of the cosmic microwave background at $z = 2.5$), $g_1 = 3$ (the degeneracy of level $n = 1$), $Z \sim 2\, T_{\rm k}/T_\circ$ (the partition function), and where $[{\rm CO/H_2}] = 10^{-4}$ is the CO abundance in typical molecular clouds (or a solar-metallicity environment; Bryant & Scoville 1996). Note that $X_{\rm CO}$ is sometimes also known as α and that we shall ignore its cumbersome units hereafter. The line luminosity, $L'_{\rm CO1-0}$, is the velocity- and area-integrated brightness temperature in the source reference frame, $L'_{\rm CO1-0} = \int_{\Delta V} \int_{A_{\rm s}} T_{\rm b}\, {\rm d}A\, {\rm d}V$, with units K km s^{-1} pc^2 (e.g. Solomon et al. 1997):

$$L'_{\rm CO1-0} = \frac{3.25 \times 10^7}{(1+z)} \left(\frac{D_{\rm lum}}{\nu_{\rm CO}} \right)^2 \int_V [S_{\rm CO1-0}\, {\rm d}V], \quad (2)$$

where $D_{\rm lum}$ is the luminosity distance in Mpc, $\nu_{\rm CO}$ is the rest-frame frequency (in GHz) of the ^{12}CO $J = 1$–0 transition and the velocity-integrated flux density is in units of Jy km s^{-1}.

Making no assumption about the state of the molecular gas, we set the minimum temperature range to $T_{\rm kin} \sim 15$–20 K, which yields $\langle X_{\rm CO}^{\rm thin} \rangle \sim 0.45$, and this can be used to compute the minimum plausible molecular gas mass in each SMG, $M_{\rm min}$ (for comparison, a temperature range of $T_{\rm kin} \sim 40$–50 K, typical of SF gas, has $\langle X_{\rm CO}^{\rm thin} \rangle \sim 0.65$). We determine $M_{\rm max}$ by adopting $X_{\rm CO} = 5$ (see Section 4.1). Note that the contribution from Helium is already included.

Setting aside issues regarding the appropriate value of $X_{\rm CO}$, it is worth mentioning that the use of CO $J = 1$–0 to estimate molecular gas masses in SMGs, rather than $J = 3$–2 or higher J lines, yields $\sim$2 times higher masses, simply because we have observed that $r_{3-2/1-0}$ is significantly below unity. If, for a moment, we adopt the so-called 'ULIRG-appropriate' value of $X_{\rm CO}$, which is around 0.8 and has been used widely to estimate molecular gas masses in SMGs (e.g. Greve et al. 2005; Tacconi et al. 2006), this would yield a median molecular gas mass of $(6.1 \pm 2.2) \times 10^{10}\,{\rm M_\odot}$ in these systems. We report the plausible range of molecular gas masses in Table 3 and now move on to discuss how best to assess the state of the molecular gas, and how we might better determine its mass, e.g. locally, the key to choosing an appropriate $X_{\rm CO}$ for ULIRGs came from dynamical constraints (Solomon et al. 1997), as we discuss in Section 4.2.

4 DISCUSSION

4.1 Physical conditions of the molecular gas

Two uncertainties plague us when we employ CO transitions to trace the mass of molecular gas in high-redshift galaxies, namely (1) the assumed $T_{\rm b}$ ratio, if transitions other than $J = 1$–0 are used, and (2) the $X_{\rm CO}$ factor, which must be appropriate for the average excitation and kinematic state of the molecular gas. The first of these has been removed by our observation of the ^{12}CO $J = 1$–0 transition, and we now focus our discussion on the second.

In practice, ^{12}CO $J = 1$–0 emission in giant molecular clouds (GMCs) can be optically thick, and $M({\rm H_2}) = X_{\rm CO}\, L'_{\rm CO1-0}$ is estimated by adopting $X_{\rm CO} \sim 5$. The latter value of $X_{\rm CO}$ was obtained from GMC studies in quiescent environments (e.g. Solomon et al. 1987; Solomon & Barrett 1991) and is robust (to within $\sim$2 times) even in warm and dense SF molecular gas, providing that the molecular gas remains reducible to ensembles of self-gravitating units in all environments [see Dickman, Snell & Schloerb (1986) for the appropriate formalism]. The failure of the latter assumption results in $X_{\rm CO} \sim 0.3$–1.3 in the extreme interstellar medium (ISM) of ULIRGs (Downes & Solomon 1998), as the molecular gas reservoir can form a continuous medium rather than an ensemble of virialized gas clumps. In the literature, $X_{\rm CO} = 0.8$ is widely adopted for SMGs, as noted earlier, but this carries a significant uncertainty, even within the ULIRG class, as the original study indicates. Such uncertainties can only be exacerbated in SMGs, e.g. more extreme

Table 3. SMG derived properties.

Name	$L'_{\rm CO1-0}$ (10^{10} K km s^{-1} pc^2)	$M_{\rm min}{}^a, M_{\rm max}{}^b$ (10^{10} M$_\odot$)	$m_{\rm CQ/SF}$	$L_{\rm IR}$ (10^{12} L$_\odot$)	$M_{\rm best}{}^c$ range (10^{10} M$_\odot$)	$M_*{}^d$ (10^{10} M$_\odot$)	$M_{\rm dyn}$ (10^{10} M$_\odot$)
SMM J123549	7.6 ± 1.0	3.4, 38	1.3	5.5 ± 1.2	2.5–7.5	21 ± 6	23 ± 4
SMM J123707-NE	2.7 ± 0.6	1.2, 13	5.0	4.1 ± 0.8	4.9–14.7	8 ± 2	18 ± 6
SMM J123707-SW	3.5 ± 0.6	1.6, 18	1.4	3.1 ± 0.6	1.5–3.5	18 ± 3	≤ 4
SMM J163650	9.3 ± 1.1	4.2, 47	0.33	7.8 ± 1.5	2.1–6.3	14 ± 4	41 ± 8
SMM J163658	10.6 ± 2.0	4.9, 54	1.5	6.4 ± 0.9	3.2–9.6	13 ± 3	58 ± 4

[a] Adopting $X_{\rm CO} = 0.45$ – see Sections 3.4 and 4.1; [b] adopting $X_{\rm CO} = 5$ – see Sections 3.4 and 4.1; [c] assuming SFE $= 500\,{\rm L_\odot\,M_\odot^{-1}}$, and plausibly up to 3 times lower – see Section 4.3; [d] from Hainline et al. (2010).

velocity fields would act to lower $X_{\rm CO}$ still further, while the presence of dominant quantities of dense [$n(\rm H_2) > 10^4\,cm^{-3}$] SF gas could increase $X_{\rm CO}$ – perhaps even back into the Galactic range. For these reasons, we do not adopt a single $X_{\rm CO}$ value, but explore its possible range, aided by the available CO lines, with the $J = 1$–0 transition now providing a normalization to the total molecular gas mass.

Since we want to avoid the assumption that the molecular gas reservoirs in SMGs are reducible to ensembles of virialized clumps, as well as being able to incorporate any information about the average state of the gas (as provided by available ^{12}CO lines), we adopt the following expression:

$$X_{\rm CO} = 2.1 \left(\frac{\sqrt{\langle n(\rm H_2)\rangle}}{T_{\rm CO1-0}} \right) K_{\rm vir}^{-1}\,{\rm M}_\odot\,\left({\rm K\,km\,s^{-1}\,pc^2}\right)^{-1}, \quad (3)$$

where $\langle n(\rm H_2)\rangle$ and $T_{\rm CO1-0}$ are the average density and $T_{\rm b}$ (in ^{12}CO $J = 1$–0) of the molecular cloud ensemble (e.g. Bryant & Scoville 1996) to be constrained by radiative transfer models of available ^{12}CO line ratios. The expression

$$K_{\rm vir} = \frac{({\rm d}V/{\rm d}r)_{\rm obs}}{({\rm d}V/{\rm d}r)_{\rm vir}} \sim 1.54 \frac{[{\rm CO/H_2}]}{\sqrt{\alpha}\,\Lambda_{\rm CO}} \left[\frac{\langle n(\rm H_2)\rangle}{10^3\,{\rm cm^{-3}}} \right]^{-1/2} \quad (4)$$

corrects $X_{\rm CO}$ for non-virial gas motions, where $\Lambda_{\rm CO} = [{\rm CO/H_2}]/({\rm d}V/{\rm d}R)$ in $({\rm km\,s^{-1}\,pc^{-1}})^{-1}$. The parameter, $\alpha = 1$–2.5, depends on the assumed density profile of a typical cloud; here we adopt an average value, $\alpha = 1.75$. Values of $K_{\rm vir} > 1$ bring $X_{\rm CO}$ towards the lower values reported for ULIRGs (Solomon et al. 1997; Downes & Solomon 1998) while $K_{\rm vir} \ll 1$ is used to exclude dynamically unattainable kinematic gas states from the range of radiative transfer modelling solutions.

We can then use ^{12}CO line ratios to constrain the average conditions of the molecular gas for the SMGs in our sample, and equation (3) to obtain the corresponding $X_{\rm CO}$ values.

For the system with the highest level of global ^{12}CO excitation, SMM J163650, our large-velocity gradient (LVG) modelling of $r_{3-2/1-0}$ and $r_{6-5/3-2}$ yields two plausible solutions, namely (i) $T_{\rm kin} \sim 20$–30 K with $n(\rm H_2) \sim 10^4$–$10^5\,cm^{-3}$ and $K_{\rm vir} \sim 4$–11, which corresponds to $\langle X_{\rm CO}\rangle \sim 4.5$ and (ii) $T_{\rm kin} \sim 90$–110 K with $n(\rm H_2) \sim 10^3\,cm^{-3}$, and $K_{\rm vir} \sim 1$, with $\langle X_{\rm CO}\rangle \sim 1$ for the corresponding gas phases. The system with the lowest excitation, SMM J123707-NE, has $r_{3-2/1-0} \sim 0.4$, which is Milky Way like and is also compatible with two ranges of LVG solutions: (i) $T_{\rm kin} = 15$ K, $n(\rm H_2) = 3 \times 10^2\,cm^{-3}$, $K_{\rm vir} \sim 1$ with $X_{\rm CO} = 10$ and (ii) $T_{\rm kin} \sim 25$ or 45–100 K, $n(\rm H_2) = (1$–$3)\times\ 10^2\,cm^{-3}$, $K_{\rm vir} \sim 4$–10 (and even up to 30) with $\langle X_{\rm CO}\rangle \sim 0.8$.

Thus $X_{\rm CO} \sim 5$–10 is certainly compatible with the global ^{12}CO line excitation observed in SMGs, as are values as low as $X_{\rm CO} \sim 0.4$–1. This dual range of LVG solutions and corresponding $X_{\rm CO}$ factors is a general characteristic of such modelling when constrained by a small number of line ratios. In our LVG models, we always find more parameter space associated with the lower rather than the higher values of $X_{\rm CO}$, but this does not make the latter less probable, nor does it help break the aforementioned degeneracy (although as we see in the following section, dynamical arguments favour the former solutions). It is important to note that the choice between the two ranges of $X_{\rm CO}$ that could apply in SMGs is not between quiescent and SF molecular gas: $X_{\rm CO} \sim 5$–10 can be associated both with cold, non-SF gas as well as with the warm, dense gas found in SF regions. Both components can be distributed widely in IR-luminous spiral galaxies and their similar $X_{\rm CO}$ factors actually ensure the robustness of global molecular gas mass estimates in such systems when using a common (usually Galactic) $X_{\rm CO}$ value (e.g. Young & Scoville 1991). Low $X_{\rm CO}$ values, on the other hand, are found in the warm, diffuse and typically non-self-gravitating gas which – for typical spirals – is confined to their nuclei (e.g. Regan 2000), and thus a low $X_{\rm CO}$ applies for only a small fraction of their total molecular gas mass. In ULIRGs, low $X_{\rm CO}$ factors (with a considerable dispersion) apply for all of their molecular gas as the aforementioned gas phase is expected to be concomitant with the entire gas reservoir (e.g. Aalto et al. 1995) – the result of high pressures in the ISM and tidal molecular cloud disruption in merger environments.

The difference between molecular gas phases with high $X_{\rm CO}$ (quiescent or SF) and those with low $X_{\rm CO}$ (found mostly in SF environments as a second phase dominating the low-J ^{12}CO emission) is mostly due to the optical depth of the ^{12}CO $J = 1$–0 line. This is large for the former ($\tau_{1-0} \gtrsim 5$) and typically small for the latter ($\tau_{1-0} \sim 0.5$–2) as a result of higher temperatures, lower densities and/or velocity gradients, with $K_{\rm vir} \gtrsim 5$. The proximity of some ULIRGs has allowed several studies to break the degeneracies (e.g. Lisenfeld, Isaak & Hills 2000; Hinz & Rieke 2006). When using low-J ^{12}CO lines this is possible with high-resolution imaging that resolves the gas discs in ULIRGs (Downes & Solomon 1998), while ^{13}CO and multi-J ^{12}CO line measurements (e.g. Mao et al. 2000; Weiß et al. 2001) that allow the mean optical depth of the ^{12}CO $J = 1$–0 line to be determined can also achieve this – see Section4.4. Finally, detailed models of CO line emission from turbulent gas clouds reveal that CO $J = 3$–2 and higher J lines are very sensitive to the presence of dense, self-gravitating cores; these lines are significantly underluminous with respect to CO $J = 1$–0 for diffuse, non-self-gravitating, turbulent gas (Ossenkopf 2002). The resulting non-linear dependence of high-J ratios such as CO $J = 7$–6/$J = 3$–2 (available for several SMGs) on the mean density of such a diffuse phase (see fig. 9 of Ossenkopf 2002) makes them unsuitable for constraining an unobserved CO $J = 1$–0 line luminosity, especially when such a phase exists alongside dense, self-gravitating, SF gas, as is the case with ULIRGs.

4.2 Dynamical constraints on $X_{\rm CO}$ and gas mass

Table 3 lists the stellar masses for our target galaxies, derived using Bruzual & Charlot stellar population models[3] (Hainline et al. 2010). We caution that these mass estimates are systematically uncertain due to the potentially complex star formation histories and dust obscuration within SMGs, as discussed by Hainline et al. (2010). We also use the measured FWHM velocity of the ^{12}CO $J = 1$–0 lines and the observed semimajor axes to determine dynamical masses, correcting for inclination using $\langle \sin^2 i\rangle = 2/3$ (following Tacconi et al. 2008). Using $M_{\rm dyn} = 2.1\sigma_{1-0}^2 R/G$ we derive a median dynamical mass within $R \sim 7$ kpc of $(2.3 \pm 1.4) \times 10^{11}\,{\rm M}_\odot$, consistent with the masses of SMGs from their resolved dynamics (Swinbank et al. 2006) and roughly 6 times more massive than UV-selected galaxies at this epoch (Erb et al. 2006), calculated in the same manner.

Combining our minimum estimate of the molecular gas mass, $\langle M_{\rm min}\rangle = (3.4 \pm 1.2) \times 10^{10}\,{\rm M}_\odot$, and the stellar masses from Hainline et al. (2010), $\langle M_*\rangle = (1.4 \pm 0.3) \times 10^{11}\,{\rm M}_\odot$, we derive a total baryonic mass, $\langle M_{\rm baryon}\rangle = (1.8 \pm 0.1) \times 10^{11}\,{\rm M}_\odot$ for our five SMGs, comparable with their median dynamical mass. We also determine a median gas mass fraction of $\langle M_{\rm min}\rangle/\langle M_{\rm baryon}\rangle = 0.14 \pm$

[3] For SMM J123707-NE, we scale the mass given by Hainline et al. (2010) for SMM J123707-SW based on the relative 5.8-μm fluxes of the components.

0.02, a median gas-to-stars mass ratio of $\langle M_{\rm min}\rangle/\langle M_*\rangle = 0.16 \pm 0.02$ and a total baryonic fraction, $f_{\rm baryon} = \langle M_{\rm baryon}\rangle/\langle M_{\rm dyn}\rangle = 0.51 \pm 0.10$. Adopting the Milky Way value for $X_{\rm CO}$ would increase the first two of these fractions by a factor of ∼10 times and would result in $f_{\rm baryon} \sim 1.5$. We note that our median baryonic mass is about 50 per cent higher than L^* at the present day (Cole et al. 2001) suggesting that SMGs are indeed the progenitors of massive galaxies.

The median baryonic mass does not exceed the median dynamical mass for $X_{\rm CO} \lesssim 3$. However, we note that the mass-to-light ratios used to derive the stellar masses are not consistent with the star formation histories implied by the observed gas mass, the current SFRs and the expectation that we are (on average) seeing the SMGs mid-way through their burst phase. If we require that SMGs are seen half-way through their burst, that the current SFR is 50 per cent efficient and is sustained for the duration of the burst, then we can use the observed dynamical masses, ^{12}CO $J = 1$–0 and rest-frame H-band luminosities to derive self-consistent constraints on $X_{\rm CO}$, the mass of the stellar population prior to the burst, and the duration of the burst. We use a constant-SFR model from STARBURST99 (Leitherer et al. 1999) to determine the mass-to-light ratio in the H band of the burst (which is obscured by a foreground dust screen with extinction, A_V) and a pre-existing, unobscured 1-Gyr stellar population whose combined luminosity is required to reproduce the observed H-band flux. A disc-like dynamical model for the molecular gas reservoir in the SMGs yields $X_{\rm CO} < 2$, an expected burst lifetime of $\lesssim$150 Myr, a gas fraction of $\lesssim$65 per cent and moderate extinction for the burst, $A_V \gtrsim 7$. In this scenario $X_{\rm CO} = 0.8$ is recovered for a model with a gas fraction of 25 per cent, a pre-existing stellar mass of $1.4 \times 10^{11}\,{\rm M}_\odot$ and a burst duration of 50 Myr with $A_V \sim 20$, which has added 20 per cent to the stellar mass of the galaxy. However, allowing a wider range of dynamical models (e.g. a virialized sphere) removes this constraint, allowing solutions as high as $X_{\rm CO} \sim 5$, and so we conclude that it is impossible with current information to reliably constrain $X_{\rm CO}$ from dynamical limits on SMG samples. Nevertheless, it is clear that values of $X_{\rm CO} \gtrsim 5$ are disfavoured.

4.3 The molecular gas in SMGs: two phases

Larger values of $X_{\rm CO}$ have the potential to radically reshape our view of the structure, gas-consumption time-scales and evolutionary state of SMGs. From their observed ^{12}CO line ratios it is obvious that they are not dominated by SF, dense and warm gas where $r_{3-2/1-0} \sim 1$ and $r_{6-5/3-2} \sim 0.8$–1, as measured for Orion A-type clouds and the central SF regions of nearby starbursts such as M 82 and NGC 253 (e.g. Wild et al. 1992; Bradford et al. 2003). For SMGs, the average value of $r_{3-2/1-0}$ is lower, with some individual sources reaching Milky Way like values, $r_{3-2/1-0} \sim 0.4$ and $r_{6-5/3-2} \sim 0.23$–0.35, well below that of SF gas.

Recalling our discussion in Section 4.1, such low ^{12}CO line ratios do not necessarily imply the presence of cold, quiescent gas such as that typifying quiescent GMCs in the Milky Way. Diffuse, warm and highly non-virial gas, concomitant with the SF phase in SMGs, can also suppress their global ^{12}CO ratios. Such a phase is responsible for the low average $r_{3-2/1-0} \sim 0.66$ in the nuclei of nearby IR-luminous galaxies (e.g. Yao et al. 2003; Leech et al. 2010) where its presence has been known for some time (Regan 2000). $r_{3-2/1-0}$ then drops from its intrinsic starburst value, ∼1, as the diffuse phase contributes extra ^{12}CO $J = 1$–0 emission, while the $J = 3$–2 and higher-J lines remain dominated by the SF gas. ^{12}CO line ratios normalized to the $J = 1$–0 line luminosity (e.g. $r_{3-2/1-0}$) would then be lower than those intrinsic to SF gas, while ratios involving only high-J lines (e.g. $r_{6-5/3-2}$) would be high, being dominated by the SF gas phase. *This is not the case for any of the SMGs in our sample* (Table 2). Moreover, LVG modelling finds no average gas state that can adequately reproduce both $r_{3-2/1-0}$ and $r_{6-5/3-2}$ for any of the SMGs in our sample, with fits of only the high-J CO ratios yielding $r_{3-2/1-0} \sim 0.9$–1.2, which is much higher than observed. Thus, while a broad two-phase differentiation of the molecular gas is certainly apparent in SMGs, *it is not of the type observed in local starburst nuclei and ULIRGs* (with its associated low $X_{\rm CO}$). Significant masses of non-SF molecular gas remain the only viable alternative for the low $r_{3-2/1-0}$ and $r_{6-5/3-2}$ observed in SMGs. This is further corroborated by the fact that the systems with the largest spatial extent of the ^{12}CO $J = 1$–0 relative to $J = 3$–2 emission show the lowest $r_{3-2/1-0}$ ratios (see Fig. 1 and Table 2).

If we assume conservatively that $X_{\rm CO}({\rm SF}) \sim X_{\rm CO}({\rm quiescent}) \sim 5$ for both the SF and quiescent gas in SMGs (in practice $X_{\rm CO}$ for the SF gas can be somewhat lower), then we arrive at robust upper limits for their total molecular gas masses, $M_{\rm max}$, as described in Section 3.4 and listed in Table 3. Alternatively, we can use $r_{3-2/1-0}$ to determine the relative fractions of cold, quiescent (CQ) and warm, SF molecular gas $m_{\rm CQ/SF} = M_{\rm CQ}/M_{\rm SF}$ from

$$m_{\rm CQ/SF} = \frac{r^{\rm (SF)}_{3-2/1-0} - r_{3-2/1-0}}{r_{3-2/1-0} - r^{\rm (CQ)}_{3-2/1-0}}, \quad (5)$$

where $r^{\rm (SF)}_{3-2/1-0} \sim 0.9$ and $r^{\rm (CQ)}_{3-2/1-0} \sim 0.3$ are set as typical intrinsic ratios of these two gas phases. The total molecular gas mass, $M_{\rm best} = M_{\rm SF}(1 + m_{\rm CQ/SF})$, can then be deduced using $L_{\rm IR}$ (Section 3.1) if we assume that the SF gas phase in all galaxies has the same intrinsic ${\rm SFE}_{\rm max} = L_{\rm IR}/M_{\rm SF}$. Its maximum value, $\sim 500\,{\rm L}_\odot\,{\rm M}_\odot^{-1}$, is thought to be the result of an Eddington limit set by photon pressure on dust in the molecular gas accreted by the SF sites (Scoville 2004; Thompson 2009) while an almost identical limiting star formation efficiency (SFE) can result from a cosmic ray generated Eddington limit (Socrates, Davis & Ramirez-Ruiz 2008). Such 'maximum SFE' values have been observed in diverse places: individual molecular clouds around OB star clusters in M 51, for the total molecular gas reservoir of Arp 220, as well as for the HCN-bright gas phase of LIRGs. Here we adopt the maximum SFE, noting that the true value will likely be smaller by a factor of up to 3 times since gas accretion towards sites of star formation may not be spherically symmetric; moreover, CO emission may also be included from beyond the natal sites of the OB stars (where the Eddington limit is set), which explains why the HCN-bright gas phase yields higher values of SFE in ULIRGs, closer to the maximum value than those associated with the CO-bright gas phase (e.g. Gao & Solomon 2004).

$m_{\rm CQ/SF}$ and $M_{\rm best}$ are listed in Table 3. Reassuringly, the maximum globally averaged ⟨SFE⟩ – estimated using $M_{\rm min}$ (via $X^{\rm thin}_{\rm CO}$) for the total gas mass and making no discrimination between SF and non-SF molecular gas – is around 160–200 $\,{\rm L}_\odot\,{\rm M}_\odot^{-1}$ for most of our SMGs, with only SMM J163650 approaching the maximum value allowed by our aforementioned arguments.

The median cold/warm gas mass fraction for the SMGs is 1.4 (Table 3). Indeed, only in one source, SMM J163650, do we find $m_{\rm CQ/SF} < 1$, strong evidence that a significant fraction of the molecular gas in most SMGs must be cold, low-excitation gas, taking no part in the starburst.[4] The large $m_{\rm CQ/SF}$ values, along with evidence for extended ^{12}CO $J = 1$–0 emission (this study; Carilli et al.

[4] Any significant AGN contribution to $L_{\rm IR}$ would lower our estimates of the warm SF molecular gas mass and increase the $m_{\rm CQ/SF}$ gas mass fractions reported in Table 3.

2010; Ivison et al. 2010a), suggest that the main gas reservoir in these systems is more widely distributed than the compact, maximal starbursts implied by high-J ^{12}CO imaging (e.g. Tacconi et al. 2006).

We consider that $M_{\rm best}$ provides the most likely range of the total molecular gas masses of the SMGs in our sample, albeit with a large uncertainty due to the plausible range of maximum SFE. Using this new method, we find a median molecular gas mass of $(2.5 \pm 0.8) \times 10^{10}\,{\rm M}_{\odot}$, with a plausible range stretching up to 3 times higher. If we combine both components in SMM J123707, this becomes $(3.2 \pm 0.9) \times 10^{10}\,{\rm M}_{\odot}$.

4.4 Breaking degeneracies in excitation and $X_{\rm CO}$ via ^{13}CO observations

During 2011–12 the EVLA will offer 2 GHz of instantaneous bandwidth, prior to commissioning of the full 8-GHz WIDAR capability. This will allow simultaneous[5] imaging of ^{12}CO and ^{13}CO $J = 1$–0, each having 4 times the velocity coverage utilized to date.

Sensitive ^{13}CO $J = 1$–0 imaging of SMGs can break the degeneracies of the ^{12}CO spectral-line energy distribution (SLED), allowing us to determine $X_{\rm CO}$ by (i) determining the total molecular gas mass via an independent, typically optically thin line or (ii) placing diagnostically powerful lower limits on the ^{12}CO/^{13}CO $J = 1$–0 line-intensity ratio, R_{1-0}. For the ^{12}CO intensities seen in our sample, deep EVLA observations can detect ^{13}CO $J = 1$–0 where $R_{1-0} \sim 3$–6, typical for cold Galactic GMCs, where ^{12}CO $J = 1$–0 is optically thick (Scoville, Solomon & Sanders 1979; Polk et al. 1988). On the other hand, the ability to set lower limits of $R_{1-0} > 10$ can decisively break the degeneracy described in Section 4.3 in favour of the diffuse phase with moderate optical depth in ^{12}CO $J = 1$–0 and low $X_{\rm CO}$. This is because while $R_{1-0} \sim 5$–10 is typical of Galactic GMCs and quiescent spiral discs (e.g. Sakamoto et al. 1997; Paglione et al. 2001), $R_{1-0} > 10$ is found almost exclusively in starbursts (e.g. Casoli, Dupraz & Combes 1992; Aalto et al. 1995) or galactic centres, where a diffuse, warm, non-self-gravitating phase dominates the $J = 1$–0 emission.

For the SMG with the lowest ^{12}CO excitation in our sample, SMM J123707-NE, our LVG models (for an abundance ratio [^{12}CO/^{13}CO] = 60) yield $R_{1-0} \gtrsim 20$ for all solutions corresponding to diffuse, warm, non-self-gravitating gas, while $R_{1-0} \sim 9$–10 is found for the dense, cold, self-gravitating phase. Similarly, for the average $r_{3-2/1-0}$ of the sample, and $R_{1-0} = 5$, all LVG solutions correspond to virial or only slightly unbound kinematic states ($K_{\rm vir} \sim 1$–3) with $X_{\rm CO} \sim 3$–6, with the best fit found for $T_{\rm k} \sim 15$ K and $n({\rm H}_2) \sim 10^3\,{\rm cm}^{-3}$ – conditions typical for quiescent GMCs. For $r_{3-2/1-0} \sim 0.6$ and $R_{1-0} \sim 15$, all solutions compatible with the aforementioned $T_{\rm b}$ ratio have $K_{\rm vir} \gtrsim 5$ and a corresponding $X_{\rm CO} \sim 0.65$–1.2. For the highest ^{12}CO $J = 1$–0 flux levels observed in our sample, a $\sim$10 times weaker ^{13}CO $J = 1$–0 line can be detected at $\gtrsim 10\,\sigma$ by the fully upgraded EVLA in $\lesssim$100 h.

Finally, we mention the possibility that there may be a significant optical depth due to dust in compact ULIRGs with very dense gas [$n({\rm H}_2) \gtrsim 10^5\,{\rm cm}^{-3}$], even at short submm wavelengths. This is suspected for nearby ULIRGs such as Arp 220, and for some SMGs (Papadopoulos et al. 2010a), and creates an additional degeneracy for the interpretation of very low (high-J)/(low-J) ^{12}CO line ratios in extreme starbursts. EVLA observations of the high-density gas tracer, HCN $J = 1$–0, at 88.632 GHz, along with low-J ^{12}CO transitions and high-J ($J = 6$–5 and higher) ^{12}CO transitions with the Atacama Large Millimetre Array (ALMA), have the potential to break this degeneracy (Papadopoulos et al. 2010b).

[5] The frequency of ^{13}CO $J = 1$–0 differs from that of ^{12}CO $J = 1$–0 by $5.070/(1 + z)$ GHz, or $\sim$1.5 GHz for the SMGs targeted here, though note that contiguous placement of sub-band pairs is not mandatory when using WIDAR.

4.5 Gas depletion time-scales and the evolutionary state of SMGs

The gas-consumption time-scale, $\tau_{\rm gas} = M({\rm H}_2)/{\rm SFR}$, is the time needed for star formation to consume a given molecular gas reservoir, in the absence of feedback effects, and can be estimated using the plausible range of values for $M_{\rm SF}$ and $M_{\rm best}$. Thus $\tau_{\rm gas}({\rm SF}) = M_{\rm SF}/{\rm SFR}$ yields the shortest feasible duration for the observed SMG bursts, while $M_{\rm best}/{\rm SFR} = \tau_{\rm gas}({\rm SF})(1 + m_{\rm CO/SF})$ is the longest time over which SF can continue if the colder material can be involved without delays imposed by dynamics or SF-related feedback.

We find a median gas-consumption time-scale, $\langle\tau_{\rm gas}({\rm SF})\rangle = 12$ Myr, which lengthens to 28 Myr if the colder gas can become involved. This is considerably shorter than naive expectations for the lifetime of the SMG phase, $\sim$300 Myr (e.g. Swinbank et al. 2006), but these gas-consumption time-scales can be extended if the SFE is below $500\,{\rm L}_{\odot}\,{\rm M}_{\odot}^{-1}$, perhaps up to 3 times longer. Moreover, we are neglecting the effect of feedback, which is also expected to lengthen the total duration of successive SF episodes in SMGs due to the need to re-accrete material towards the typically very compact SF regions ($\sim$100–500 pc) expected in merger-driven, gas-rich starbursts.

4.6 The rest-frame Schmidt–Kennicutt relation in the distant Universe: a comparison to the local Universe

The availability of a significant number of ^{12}CO $J = 1$–0 line luminosities in vigorously SF systems at high redshifts presents an opportunity to examine the Schmidt–Kennicutt (S–K) relation between their gas reservoirs and SFRs, without resorting to the use of high-J ^{12}CO transitions and assumptions about global ^{12}CO high-J/$J = 1$–0 line ratios (i.e. assumptions about the average state of their molecular gas reservoirs). The latter can create artificial offsets from the S–K relation for galaxy populations where only high-J ^{12}CO lines have been observed, if an incorrect ^{12}CO high-J/$J = 1$–0 ratio is assumed. Such offsets can also be created by the application of inappropriate $X_{\rm CO}$ factors in various galaxy classes. For our present short discussion we render the S–K relation only as a $L_{\rm IR}$–$L'_{\rm CO}$ relation, postponing our investigation of the physical relation, SFR–$M({\rm H}_2)$, where $X_{\rm CO}$ must be considered, for a future paper (Greve et al., in preparation) .

In its original form, the S–K relation was established via H I and ^{12}CO $J = 1$–0 measurements of galaxies in the local Universe (Schmidt 1959; Kennicutt 1989, 1998b). The H I + H_2 gas surface densities, $\Sigma({\rm H\,I}+{\rm H}_2)$, are related to the star formation surface density, $\Sigma_\star$, by $\Sigma_\star \propto [\Sigma({\rm H\,I} + {\rm H}_2)]^\kappa$, where $\kappa \sim 1.4$–1.5. In a recent, comprehensive analysis of the H I and H_2 distributions in nearby galaxies, on sub-kpc scales, Bigiel et al. (2009) found a power law with slope $N = 1.0 \pm 0.2$ in regions where the total gas content (H I + H_2) is dominated by H_2. The latter seems to be characterized by gas surface densities $\gtrsim 9\,{\rm M}_{\odot}\,{\rm pc}^{-2}$, indicating a saturation point for H I.

Assuming that distant LIRGs are mostly H I-poor, as they are in the local Universe, with $\lesssim$20 per cent of the their total gas in H I, we

can estimate their total mass using the ^{12}CO $J = 1$–0 line. Even for the most H I-rich local LIRGs, omission of H I results in a gas-mass underestimate of $\lesssim$2 times, leaving $X_{\rm CO}$ as the dominant uncertainty (see Section 4.1).

That SMGs follow the S–K relation in its basic observational form, $L_{\rm IR}$–$L'_{\rm CO}$, was first shown by the ^{12}CO $J = 3$–2 and 4–3 survey of SMGs by Greve et al. (2005). More recently, CO surveys of gas-rich disc galaxies at $z = 1$–2 (Daddi et al. 2008, 2010; Dannerbauer et al. 2009; Genzel et al. 2010) have shown that they too obey a S–K-like relation, albeit apparently offset from the SMGs (lower $L_{\rm IR}/L'_{\rm CO}$). It has been speculated that this offset reflects two modes of global star formation in galaxies: SMGs typify those galaxies undergoing major mergers, with intense, highly efficient bursts of star formation, and BzKs typify galaxies undergoing a more leisurely rate of star formation, at lower efficiency. However, this apparent offset in the S–K relation is deduced from a comparison of high-J CO observations from SMGs with a mixture of CO $J = 3$–2, $J = 2$–1 and 1−0 line observations of disc galaxies, and the reality of the apparent offset (and its interpretation as different global star-formation laws for mergers and disc galaxies) is therefore hampered by biases and uncertainties in the underlying gas excitation, especially in SMGs.

With an increased sample of SMGs observed in ^{12}CO $J = 1$–0, we can make a relatively unbiased comparison between SMGs and the $z \sim 1$–2 disc population. In Fig. 2 we show $L_{\rm IR}$ (Section 3.1) versus $L'_{\rm CO1-0}$, populated with local LIRGs and ULIRGs from Papadopoulos et al. (in preparation) as well as with those SMGs and BzK galaxies with reliable measurements of ^{12}CO $J = 1$–0 or $J = 2$–1 (where $J = 1$–0 is not available, we use $J = 2$–1, calculating $L'_{\rm CO1-0}$ via $r_{21} = 0.75$). We see that the SMGs extend the S–K relation to higher luminosities, with a low dispersion. Fitting linear relations of the form $\log L_{\rm IR} = \alpha \log L'_{\rm CO1-0} + \beta$, we determine slopes for the various samples, reporting these in the labels of Fig. 2. Taking the SMGs alone, we find $\alpha = 0.65 \pm 0.13$ and $\beta = 5.7 \pm 1.4$; local ULIRGs display a shallower slope, $\alpha = 0.39 \pm 0.11$ with $\beta = 8.4 \pm 1.1$, though this is highly uncertain as they span only a small range in $L_{\rm IR}$; for LIRGs we see $\alpha = 0.67 \pm 0.05$ and $\beta = 5.0 \pm 0.5$, similar to the SMGs.

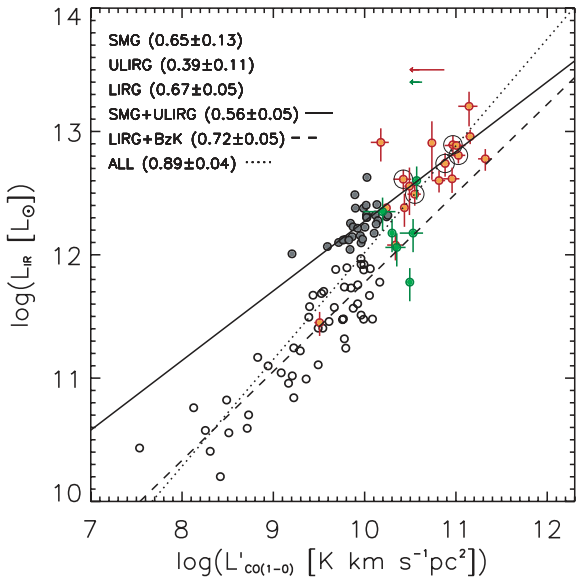

Figure 2. $L_{\rm IR}$ versus $L'_{\rm CO}$ for those SMGs, local (U)LIRGs and BzK galaxies (see legend) with robust CO $J = 1$–0 (or $J = 2$–1) measurements. Trend lines are fitted to the ULIRGs plus SMGs (solid) and LIRGs plus BzK galaxies (dashed), as well as all the samples combined (dotted). The resulting linear slopes are given in parentheses. Also shown are the mean corrections that would have been required in $L'_{\rm CO}$ for the SMGs (and BzK galaxies) if their CO luminosities had been derived using CO $J = 3$–2 (or $J = 2$–1), which would have resulted in an erroneously steep trend. The measurements from this paper are circled.

Generally, we find slopes that are significantly below unity ($\alpha \sim 0.5$–0.7) for the various samples. This contrasts with the steeper slopes ($\alpha \sim 1.1$–1.5) reported by other studies of low- and high-redshift samples (e.g. Greve et al. 2005; Daddi et al. 2010; Genzel et al. 2010). These have typically employed high-J ^{12}CO line luminosities for the high-redshift galaxies and $L'_{\rm CO1-0}$ for the local sources, which may artificially steepen the slope. Iono et al. (2009) looked at the S–K relation using ^{12}CO $J = 3$–2 for both low- and high-redshift galaxies, finding $\alpha = 1.08 \pm 0.03$, similar to that derived by Gao & Solomon (2004) using HCN $J = 1$–0. These two molecular transitions both trace the dense, warm, SF gas phase. A common slope of unity in the corresponding S–K relations is to be expected if a near-constant $\mathrm{SFE_{max}} = L_{\rm IR}/M_{\rm SF}$ underlies star formation in all galaxies, with only the dense gas phase available as fuel, and an Eddington-type limit (set by photons or cosmic rays) setting $\mathrm{SFE_{max}}$ (see Section 4.3).

Taking the SMGs and ULIRGs together – they both contain extreme SF environments, after all – yields $\alpha = 0.56 \pm 0.05$ and $\beta = 6.6 \pm 0.6$, whereas taking the LIRGs and BzK galaxies together yields $\alpha = 0.72 \pm 0.05$ and $\beta = 4.6 \pm 0.5$. The BzK galaxies do not stand out dramatically from the other low- and high-redshift samples. There are only three BzK galaxies with ^{12}CO $J = 1$–0 detections (Aravena et al. 2010), but the situation is unchanged when we include the BzK galaxies detected in ^{12}CO $J = 2$–1 from Daddi et al. (2010), adopting $r_{2-1/1-0} = 0.75$ to calculate $L'_{\rm CO1-0}$. If, however, we compare the BzKs with the SMGs, this time using the ^{12}CO $J = 3$–2, 4–3 and 5–4 lines for the latter (the mean resulting offset in $L'_{\rm CO}$ is shown in Fig. 2), then one might argue that SMGs and ULIRGs populate a different sequence to BzK and spiral galaxies, as did Daddi et al. (2010). Thus an apparent displacement and/or steepening of the S–K relation between various galaxy populations may not reflect a true difference in their respective SF modes, but rather the strong excitation biases produced by using molecular lines with different excitation requirements. Given these biases, the relatively small galaxy samples, and their scatter, the evidence for different S–K relations between different galaxy populations is weak, as we shall argue in a forthcoming paper (Greve et al., in preparation).

Adding a last cautionary note, Papadopoulos & Pelupessy (2010) have shown that while typical present-day galaxies quickly settle into S–K type relations, this may not be the case for gas-rich, metal-poor systems in the early Universe. Such galaxies can spend sustained periods with their SFR significantly below or above that expected from the local S–K relation. If the same gas-rich, metal-poor galaxy can deviate strongly from the S–K relation during the course of its evolution, then the use of the S–K relation as a tool for differentiating between different SF modes must be re-evaluated. Indeed, given the dynamic and non-equilibrium ISM in strongly evolving, gas-rich systems [where the global mass fractions of the various gas phases, e.g. $M_{\rm SF}({\rm H_2})/M_{\rm total}$ and $M({\rm H\,I})/M({\rm H_2})$, are strongly time-dependent] there could be a simple, underlying S–K relation of SFR $\propto M_{\rm SF}({\rm H_2})$, while the different exponents recovered in various samples are artefacts of strongly evolving $M_{\rm SF}({\rm H_2})/M_{\rm total}$ fractions, further compounded by the choice of observed molecular lines so with different excitation requirements for high-redshift systems.

5 FUTURE PROSPECTS

5.1 Blind surveys

Blain, Carilli & Darling (2004) present the number of blind CO $J = 1$–0 line detections expected with 4-GHz wide observing bands, based on Blain et al. (2002), updating the work of Carilli & Blain (2002) to reflect the SMG redshift distribution of Chapman et al. (2005). Their 30–34 GHz band is most easily compared with our $z \sim 2.4$ SMGs: scaling to our 236 MHz of instantaneous bandwidth, they predict a source density of $\sim$2.4 deg^{-2} at the flux levels (Section 2) to which we are sensitive, $\gtrsim 2 \times 10^{-22}$ W m^{-2} or $\gtrsim$0.18 Jy km s^{-1}.

It is no great surprise, therefore, that we find no robust ($>5\,\sigma$) detections within the four fields of our pilot survey, each with a $\sim$70-arcsec FWHM primary beam: sensitivities ranging from $\sim$0.1–0.2 Jy km s^{-1}, covering $\sim 10^{-3}$ deg^2.

In Blain et al., the galaxies responsible for $J = 1$–0 emission at or above the level to which we are sensitive are extremely luminous – they have higher $L_{\rm IR}$ than our SMGs. This suggests the predictions may be rather pessimistic; of course, we might also expect to see an overdensity of sources since our fields are centred on relatively massive galaxies (e.g. Stevens et al. 2003).

Based on the predictions of Blain et al., a blind survey utilizing WIDAR's full 8-GHz bandwidth, would need to cover $\sim$100 times our current area, to a similar depth, to provide a significant number of robust detections and hence a useful test of the predictions. Our survey suggests these requirements can be relaxed significantly; it will be interesting to see whether the $\sim$2 times deeper observations planned for our targets using EVLA's C configuration provide evidence to support our suggestion.

5.2 The study of cold, quiescent molecular gas at high redshift

All current molecular-lines studies of distant starbursts, including our own, involve samples selected via large rest-frame far-IR luminosities and luminous high-J ^{12}CO lines ($J = 3$–2 and higher). It is thus possible that SMGs with low $r_{3-2/1-0}$ ratios remain mostly undetected by the ^{12}CO $J = 3$–2 surveys and were thereby excluded from our study, as noted in Section 3.3.

The fact that much of the molecular gas in SF systems may not be participating in the starbursts has been well established by studies of local LIRGs, where sensitive low-J ^{12}CO imaging (e.g. Weiß, Walter & Scoville 2004) or submm continuum imaging of dust (e.g. Papadopoulos & Seaquist 1999; Dunne & Eales 2001; Thomas et al. 2002) could *spatially* disentangle the cold and extended molecular gas and/or its associated dust from the compact starbursts, which otherwise dominate their global SEDs and their molecular SLEDs.

It has only recently become possible to attempt a similar spatial separation of ISM components in high-redshift systems, via tracers that can remain luminous in the cold, low-excitation ISM – e.g. ^{12}CO $J = 1$–0 and submm continuum emission from dust. This explains the previous lack of evidence for extended, low-excitation molecular gas around SMGs, but also point to several obvious routes forward, via EVLA and ALMA.

Less well known is the prospect of utilizing the two fine-structure lines of neutral carbon, $^3P_1 \rightarrow {}^3P_0$ at 492.160 GHz and $^3P_2 \rightarrow {}^3P_1$ at 809.343 GHz to trace molecular gas and dynamical mass (Papadopoulos, Thi & Viti 2004; Papadopoulos & Greve 2004; Weiß et al. 2005a), exploiting the full concomitance of C and CO in molecular clouds (Keene et al. 1996), the simple, three-level partition function, the low optical depth and modest excitation requirements. Moreover, unlike the luminous [C II] fine-structure line at 1.9 THz, the neutral carbon lines are not subject to contamination by atomic or ionized gas, tracing solely the molecular gas. The [C I] $J = 1$–0 line remains luminous even for UV-shielded, cold ($T_{\rm k} \sim 15$ K) molecular gas (e.g. Oka et al. 2001) where the [C II] line luminosity is negligible because all carbon is neutral and $T_{\rm k} \ll \Delta E_{\rm u}([{\rm C\,II}])/k_{\rm B} \sim 92$ K. Finally, the [C I] lines are accessible in the most sensitive bands (3–7 or 84–373 GHz) of ALMA for a much wider redshift range (and range of look-back times) than [C II] – $z \sim 0.3$–4.9 for $J = 1$–0 and $z \sim 1.2$–8.6 for $J = 2$–1 versus $z \gtrsim 4$ for [C II].

The [C I] $^3P_1 \rightarrow {}^3P_0$ line, in particular, remains well excited in quiescent GMCs ($E_{\rm u}/k_{\rm B} \sim 24$ K, $n_{\rm crit} \sim 600$ cm^{-3} for low $T_{\rm k}$), while maintaining a favourable K-correction with respect to ^{12}CO $J = 1$–0 [$S_{\rm CI}/S_{\rm CO} \sim 2.75$–5.5 for $T_{\rm b}([{\rm C\,I}])/T_{\rm b}({\rm CO}) \sim 0.15 - 0.30$]. The $^3P_2 \rightarrow {}^3P_1$ line ($E_{\rm u}/k_{\rm B} \sim 63$ K, $n_{\rm crit} \sim 965$ cm^{-3}) also maintains a K-correction advantage with respect to both ^{12}CO $J = 1$–0 and $J = 7$–6 (the CO line closest in rest-frame frequency), while detecting the pair yields an excellent thermometer for molecular gas (both lines are available in bands 3–7 of ALMA for $z \sim 1.2$–4.9). Thus [C I] $J = 1$–0, $J = 2$–1 imaging with ALMA and CO $J = 1$–0 imaging with the completed EVLA will constitute the most powerful tools for making inventories of the global molecular gas and dynamical gas mass in distant galaxies, unbiased by the excitation state of the molecular gas and the extent of their star formation regions.

6 CONCLUSIONS

We report the results of a pilot study with the EVLA of ^{12}CO $J = 1$–0 emission from a small sample of well-studied SMGs at $z = 2.2$–2.5, previously detected in ^{12}CO $J = 3$–2 using PdBI.

Using the EVLA's most compact configuration we detect strong, broad ($\sim$1000 km s^{-1} FWZI) line emission from all of our targets – coincident in position and velocity with their $J = 3$–2 emission.

The median linewidth ratio, $\sigma_{1-0}/\sigma_{3-2} = 1.15 \pm 0.06$, suggests that the $J = 1$–0 emission is more spatially extended than the $J = 3$–2 emission, a situation confirmed by our maps which reveal velocity structure in several cases and typical sizes of $\sim$16 kpc FWHM. With the current spatial resolution, we are unable to determine whether observed gas motions are well ordered, but we find no evidence of large-scale flows of cold gas.

We find a median $T_{\rm b}$ ratio of $r_{3-2/1-0} = 0.55 \pm 0.05$, consistent with local galaxies with $L_{\rm IR} > 10^{11}$ L$_\odot$, noting that our value may be biased high because of the $J = 3$–2 based sample selection. Including five systems with similar luminosities from the literature, we find a median of $r_{3-2/1-0} = 0.58 \pm 0.05$ and see no evidence for measurable intrinsic scatter within the sample.

Using the observed ^{12}CO $J = 1$–0 line emission, naive estimates of the molecular gas masses are around 2 times higher than previous estimates based on ^{12}CO $J = 3$–2 with $r_{3-2/1-0} = 1$.

We also estimate molecular gas masses using the ^{12}CO $J = 1$–0 line and the observed global $T_{\rm b}$ ratios, assuming standard underlying $T_{\rm b}$ ratios for the non-SF and SF gas phases as well as a common SFE for the latter in all systems, i.e. without calling upon $X_{\rm CO}$. Using this new method, we find a median molecular gas mass of $(2.5 \pm 0.8) \times 10^{10}$ M$_\odot$, with a plausible range stretching up to 3 times higher. Even higher masses cannot be ruled out, but are not favoured by dynamical constraints: the median dynamical mass within $R \sim 7$ kpc for our sample, $(2.3 \pm 1.4) \times 10^{11}$ M$_\odot$, $\sim$6 times more massive than UV-selected galaxies at this epoch.

We find a median gas-consumption time-scale, $\langle \tau_{\rm gas}({\rm SF}) \rangle = 12$ Myr, or 28 Myr if the colder gas can become involved. This is shorter than naive expectations for the lifetime of the SMG phase,

but these time-scales can be longer if the SFE is below 500 $L_\odot\,M_\odot^{-1}$, and we neglect the effect of feedback.

We examine the S–K relation in $L_{\rm IR}$–$L'_{\rm CO}$ for all the distant galaxy populations for which CO $J = 1$–0 or $J = 2$–1 data are available, finding small systematic differences between populations. These have previously been interpreted as evidence for different modes of star formation, but we argue that these differences are to be expected, given the still considerable uncertainties, certainly when considering the probable excitation biases due to the molecular lines used, and the possibility of sustained S–K offsets during the evolution of individual, gas-rich systems.

We discuss the degeneracies surrounding molecular gas mass estimates, the possibilities for breaking them and the future prospects for imaging and studying cold, quiescent molecular gas at high redshift.

We note in ending that if SMGs (and other high-redshift starbursts) are as extended as our observations suggest (up to 20 kpc) then even the shortest possible dish spacings of the EVLA are not well matched to their sizes. However, the smaller ALMA dishes (especially those in the ALMA Compact Array), if fitted with Band-1 receivers, or GBT, are ideal for studying the critical ^{12}CO $J = 1$–0 emission from these galaxies.

ACKNOWLEDGMENTS

We would like to express our immense gratitude to the EVLA commissioning team and all those that have helped to create this remarkable facility. We thank Andy Harris, Andrew Baker and Mark Swinbank for useful discussions, an anonymous referee for comments that improved our paper significantly, and Mrs Katerina Papadopoulos for her visit to Pasadena. IS acknowledges support from STFC.

REFERENCES

Aalto S., Booth R. S., Black J. H., Johansson L. E. B., 1995, A&A, 300, 369
Aravena M. et al., 2010, ApJ, 718, 177
Bigiel F., Walter F., Leroy A., Brinks E., de Blok W., Madore B., Thornley M., 2009, in Sheth K., Noriega-Crespo A., Ingalls J., Paladini R., eds, The Evolving ISM in the Milky Way and Nearby Galaxies, Spitzer Science Center, Pasadena: ssc.spitzer.caltech.edu/mtgs/ismevol
Blain A. W., Smail I., Ivison R. J., Kneib J., Frayer D. T., 2002, Phys. Rep., 369, 111
Blain A. W., Carilli C., Darling J., 2004, New Astron. Rev., 48, 1247
Borys C., Chapman S., Halpern M., Scott D., 2003, MNRAS, 344, 385
Bothwell M. S. et al., 2010, MNRAS, 405, 219
Bradford C. M., Nikola T., Stacey G. J., Bolatto A. D., Jackson J. M., Savage M. L., Davidson J. A., Higdon S. J., 2003, ApJ, 586, 891
Bryant P. M., Scoville N. Z., 1996, ApJ, 457, 678
Carilli C. L., Blain A. W., 2002, ApJ, 569, 605
Carilli C. L. et al., 2010, ApJ, 714, 1407
Casoli F., Dupraz C., Combes F., 1992, A&A, 264, 55
Chapman S. C., Blain A. W., Ivison R. J., Smail I. R., 2003, Nat, 422, 695
Chapman S. C., Blain A., Smail I., Ivison R., 2005, ApJ, 622, 772
Cole S. et al., 2001, MNRAS, 326, 255
Daddi E., Dannerbauer H., Elbaz D., Dickinson M., Morrison G., Stern D., Ravindranath S., 2008, ApJ, 673, L21
Daddi E. et al., 2010, ApJ, 714, L118
Danielson A. L. R. et al., 2010, MNRAS, doi:10.1111/j.1365-2966.2010.17549.x
Dannerbauer H., Daddi E., Riechers D. A., Walter F., Carilli C. L., Dickinson M., Elbaz D., Morrison G. E., 2009, ApJ, 698, L178
Davies M. L. et al., 2009, MNRAS, 400, 984
Dekel A., Sari R., Ceverino D., 2009, ApJ, 703, 785
Dickman R. L., Snell R. L., Schloerb F. P., 1986, ApJ, 309, 326
Downes D., Solomon P. M., 1998, ApJ, 507, 615
Downes D., Solomon P. M., 2003, ApJ, 582, 37
Dunne L., Eales S. A., 2001, MNRAS, 327, 697
Erb D. K., Steidel C. C., Shapley A. E., Pettini M., Reddy N. A., Adelberger K. L., 2006, ApJ, 646, 107
Franzen T. M. O. et al., 2009, MNRAS, 400, 995
Frayer D. T., Ivison R. J., Scoville N. Z., Yun M., Evans A. S., Smail I., Blain A. W., Kneib J., 1998, ApJ, 506, L7
Frayer D. T. et al., 1999, ApJ, 514, L13
Frayer D. T. et al., 2008, ApJ, 680, L21
Frayer D. T. et al., 2010 preprint (arXiv e-prints)
Gao Y., Solomon P. M., 2004, ApJS, 152, 63
Genzel R., Baker A. J., Tacconi L. J., Lutz D., Cox P., Guilloteau S., Omont A., 2003, ApJ, 584, 633
Genzel R. et al., 2010, MNRAS, 407, 2091
Greve T. R., Ivison R. J., Papadopoulos P. P., 2003, ApJ, 599, 839
Greve T. R. et al., 2005, MNRAS, 359, 1165
Hainline L. J., Blain A. W., Greve T. R., Chapman S. C., Smail I., Ivison R. J., 2006, ApJ, 650, 614
Hainline L. J., Blain A. W., Smail I., Alexander D. M., Armus L., Chapman S. C., Ivison R. J., 2010, MNRAS, preprint (arXiv:1006.0238)
Harris A. I., Baker A. J., Zonak S. G., Sharon C. E., Genzel R., Rauch K., Watts G., Creager R., 2010, ApJ, 723, 1139
Hinz J. L., Rieke G. H., 2006, ApJ, 646, 872
Iono D. et al., 2009, ApJ, 695, 1537
Ivison R. J., Smail I., Barger A. J., Kneib J., Blain A. W., Owen F. N., Kerr T. H., Cowie L. L., 2000, MNRAS, 315, 209
Ivison R. J., Smail I., Frayer D. T., Kneib J., Blain A. W., 2001, ApJ, 561, L45
Ivison R. J. et al., 2002, MNRAS, 337, 1
Ivison R. J. et al., 2008, MNRAS, 390, 1117
Ivison R. J., Smail I., Papadopoulos P. P., Wold I., Richard J., Swinbank A. M., Kneib J., Owen F. N., 2010a, MNRAS, 404, 198
Ivison R. J. et al., 2010b, A&A, 518, L35
Keene J., Lis D. C., Phillips T. G., Schilke P., 1996, in van Dishoeck E. F., ed., IAU Symp. 178, Molecules in Astrophysics: Probes & Processes. Kluwer, Dordrecht, p. 129
Kennicutt R. C., Jr, 1989, ApJ, 344, 685
Kennicutt R. C., Jr, 1998a, ARA&A, 36, 189
Kennicutt R. C., Jr, 1998b, ApJ, 498, 541
Kneib J., Neri R., Smail I., Blain A., Sheth K., van der Werf P., Knudsen K. K., 2005, A&A, 434, 819
Knudsen K. K., Neri R., Kneib J., van der Werf P. P., 2009, A&A, 496, 45
Leech J., Isaak K. G., Papadopoulos P. P., Gao Y., Davis G. R., 2010, MNRAS, 406, 1364
Leitherer C. et al., 1999, ApJS, 123, 3
Lilly S. J., Eales S. A., Gear W. K. P., Hammer F., Le Fèvre O., Crampton D., Bond J. R., Dunne L., 1999, ApJ, 518, 641
Lisenfeld U., Isaak K. G., Hills R., 2000, MNRAS, 312, 433
Mao R. Q., Henkel C., Schulz A., Zielinsky M., Mauersberger R., Störzer H., Wilson T. L., Gensheimer P., 2000, A&A, 358, 433
Morrison G. E., Owen F. N., Dickinson M., Ivison R. J., Ibar E., 2010, ApJS, 188, 178
Neri R. et al., 2003, ApJ, 597, L113
Oka T. et al., 2001, ApJ, 558, 176
Ossenkopf V., 2002, A&A, 391, 295
Paglione T. A. D. et al., 2001, ApJS, 135, 183
Papadopoulos P. P., Greve T. R., 2004, ApJ, 615, L29
Papadopoulos P. P., Ivison R. J., 2002, ApJ, 564, L9
Papadopoulos P. P., Pelupessy F. I., 2010, ApJ, 717, 1037
Papadopoulos P. P., Seaquist E. R., 1999, ApJ, 514, L95
Papadopoulos P. P., Thi W., Viti S., 2004, MNRAS, 351, 147
Papadopoulos P. P., van der Werf P., Isaak K., Xilouris E. M., 2010a, ApJ, 715, 775
Papadopoulos P. P., Isaak K., van der Werf P., 2010b, ApJ, 711, 757
Polk K. S., Knapp G. R., Stark A. A., Wilson R. W., 1988, ApJ, 332, 432
Pope A. et al., 2008, ApJ, 675, 1171

Regan M. W., 2000, ApJ, 541, 142
Sakamoto S., Handa T., Sofue Y., Honma M., Sorai K., 1997, ApJ, 475, 134
Schinnerer E. et al., 2008, ApJ, 689, L5
Schmidt M., 1959, ApJ, 129, 243
Scott S. E. et al., 2002, MNRAS, 331, 817
Scoville N., 2004, in Aalto S., Huttemeister S., Pedlar A., eds, ASP Conf. Ser. Vol. 320, The Neutral ISM in Starburst Galaxies. Astron. Soc. Pac., San Francisco, p. 253
Scoville N. Z., Solomon P. M., Sanders D. B., 1979, in Burton W. B., ed., IAU Symp. 84, The Large-Scale Characteristics of the Galaxy. Reidel, Dordrecht, p. 277
Smail I., Chapman S. C., Ivison R. J., Blain A. W., Takata T., Heckman T. M., Dunlop J. S., Sekiguchi K., 2003, MNRAS, 342, 1185
Smail I., Chapman S. C., Blain A. W., Ivison R. J., 2004, ApJ, 616, 71
Socrates A., Davis S. W., Ramirez-Ruiz E., 2008, ApJ, 687, 202
Solomon P. M., Barrett J. W., 1991, in Combes F., Casoli F., eds, IAU Symp. 146, Dynamics of Galaxies and Their Molecular Cloud Distributions. Kluwer, Dordrecht, p. 235
Solomon P. M., Vanden Bout P. A., 2005, ARA&A, 43, 677
Solomon P. M., Rivolo A. R., Barrett J., Yahil A., 1987, ApJ, 319, 730
Solomon P. M., Downes D., Radford S. J. E., Barrett J. W., 1997, ApJ, 478, 144
Stevens J. A. et al., 2003, Nat, 425, 264
Swinbank A. M., Chapman S. C., Smail I., Lindner C., Borys C., Blain A. W., Ivison R. J., Lewis G. F., 2006, MNRAS, 371, 465
Swinbank A. M. et al., 2008, MNRAS, 391, 420
Swinbank A. M. et al., 2010, Nat, 464, 733
Tacconi L. J. et al., 2006, ApJ, 640, 228
Tacconi L. J. et al., 2008, ApJ, 680, 246
Thomas H. C., Dunne L., Clemens M. S., Alexander P., Eales S., Green D. A., James A., 2002, MNRAS, 331, 853
Thompson T. A., 2009, in Wang W., Yang Z., Luo Z., Chen Z., eds, ASP Conf. Ser. Vol. 408, The Starburst-AGN Connection. Astron. Soc. Pac., San Francisco, p. 128
Walter F., Weiss A., Scoville N., 2002, ApJ, 580, L21
Wardlow J. L. et al., 2010, preprint (arXiv e-prints)
Weiß A., Neininger N., Hüttemeister S., Klein U., 2001, A&A, 365, 571
Weiß A., Walter F., Scoville N., 2004, in Aalto S., Huttemeister S., Pedlar A., eds, ASP Conf. Ser. Vol. 320, The Neutral ISM in Starburst Galaxies. Astron. Soc. Pac., San Francisco, p. 142
Weiß A., Downes D., Henkel C., Walter F., 2005a, A&A, 429, L25
Weiß A., Walter F., Scoville N. Z., 2005b, A&A, 438, 533
Weiß A., Ivison R. J., Downes D., Walter F., Cirasuolo M., Menten K. M., 2009, ApJ, 705, L45
Wild W., Harris A. I., Eckart A., Genzel R., Graf U. U., Jackson J. M., Russell A. P. G., Stutzki J., 1992, A&A, 265, 447
Yao L., Seaquist E. R., Kuno N., Dunne L., 2003, ApJ, 588, 771
Young J. S., Scoville N. Z., 1991, ARA&A, 29, 581

This paper has been typeset from a TEX/LATEX file prepared by the author.